This is a repository copy of *Mineralogy of sulfides*.

White Rose Research Online URL for this paper:
http://eprints.whiterose.ac.uk/113362/

Version: Published Version

Article:

Mineralogy of Sulfides

David J. Vaughan[1] and Claire L. Corkhill[2]

Metal sulfides are the most important group of ore minerals. Here, we review what is known about their compositions, crystal structures, phase relations and parageneses. Much less is known about their surface chemistry, their biogeochemistry, or the formation and behaviour of 'nanoparticle' sulfides, whether formed abiotically or biogenically.

KEYWORDS: metal sulfides, crystal structures, paragenesis, surface chemistry, biogeochemistry

INTRODUCTION

Sulfide minerals are compounds in which sulfur is combined as an anion with a metal (or semi-metal) cation or cations. The definition is commonly widened to include minerals in which the anion is As or Sb, sometimes together with S, and to include Se and Te minerals. The sulfosalts are a special group of the sulfide minerals that have a general formula $A_mT_nX_p$ and in which the common elements are A = Ag, Cu, Pb; T = As, Sb, Bi; X = S. They generally contain pyramidal TS_3 groups in their structures. Several hundred sulfide minerals are known, but only five are sufficiently abundant accessory minerals to have been categorized as 'rock forming' (Bowles et al. 2011). These five are pyrite, pyrrhotite, galena, sphalerite and chalcopyrite, and it is the iron sulfides (pyrite and pyrrhotite) which are dominant. The very fine particulate iron sulfides found in reducing environments beneath the surfaces of some sediments and soils are also important. Formerly known as 'amorphous iron sulfides', they are now known to be mackinawite (tetragonal FeS) and, to a lesser extent, greigite (Fe_3S_4). Both mackinawite and greigite are metastable compared to pyrite and pyrrhotite.

Above all, the sulfides are the most important group of ore minerals because they are responsible for the concentration of a wide range of metals as mineable deposits. They are also potential sources of pollution, be it of the air, surface waters, or soils. Air pollution may arise both from the smelting of sulfide ores and from the burning of coal, which contains sulfur mainly as sulfide impurities. The breakdown of sulfides exposed by weathering at the Earth's surface generates sulfuric acid, as well as releasing potentially toxic metals into waters and soils. This form of pollution may arise from mine wastes (*acid mine drainage*) or sulfide-containing natural rocks (*acid rock drainage*).

1 School of Earth, Atmospheric and Environmental Sciences, and Williamson Research Centre for Molecular Environmental Science University of Manchester Manchester M13 9PL, UK E-mail: david.vaughan@manchester.ac.uk

2 NucleUS Immobilisation Science Laboratory Department of Materials Science and Engineering University of Sheffield Sheffield S1 3JD, UK E-mail: c.corkhill@sheffield.ac.uk

The literature on sulfide minerals is extensive, with a number of overview textbooks and monographs. Comprehensive reviews can be found in Ribbe (1974), Vaughan and Craig (1978), and, most recently, in Vaughan (2006). The present article provides a brief overview of the compositions and crystal structures of the major sulfide minerals, aspects of their chemistries (bulk and surface) and their occurrence. In addition to the sulfides mentioned above, pentlandite [$(Fe,Ni)_9S_8$] and its alteration product, violarite ($FeNi_2S_4$), are important as the major ore minerals of nickel; bornite (Cu_5FeS_4) and chalcocite (Cu_2S) as major copper minerals; and molybdenite (MoS_2) is the primary source of molybdenum. Tetrahedrite ($Cu_{12}Sb_4S_{13}$) is notable because of the large range of metals, silver in particular, which can substitute at percent levels for copper or antimony in its structure. In contrast, arsenopyrite (FeAsS) is the major natural source of arsenic, an extremely toxic pollutant.

CRYSTAL STRUCTURES AND THE CLASSIFICATION OF SULFIDES

The most important sulfides are categorized into groups based on major structure types or having key structural features in common (TABLE 1) (see Makovicky 2006 for detailed classification). Commonly, these are the structures exhibited by a much larger group of crystalline solids, such as the rocksalt structure of the galena group (FIG. 1A), the sphalerite and wurtzite forms of ZnS (FIGS. 1B, 1C), or the nickel arsenide structure (FIG. 1D).

The disulfide group of minerals (FIG. 1E) contain dianion units (S–S, S–As, As–As, etc.). In the pyrite structure, FeS_6 octahedra share corners along the *c*-axis direction, whereas in the marcasite form of FeS_2, the octahedra share edges to form chains of octahedra along the *c*-axis. Loellingite ($FeAs_2$) and arsenopyrite (FeAsS) are variants of the marcasite structure with, respectively, shorter or alternately long and short metal–metal distances across the shared octahedral edge.

Sulfides such as covellite (CuS) (FIG. 1F) and molybdenite (MoS_2) have layer structures; other sufides have structures that are best described by rings or chains of linked atoms [such as realgar (AsS)]. A diverse group, defined as the metal-excess group by Vaughan and Craig (1978), have metal:sulfur ratios greater than 1:1 and structures of the type illustrated by pentlandite, the major ore mineral of nickel (FIG. 1G).
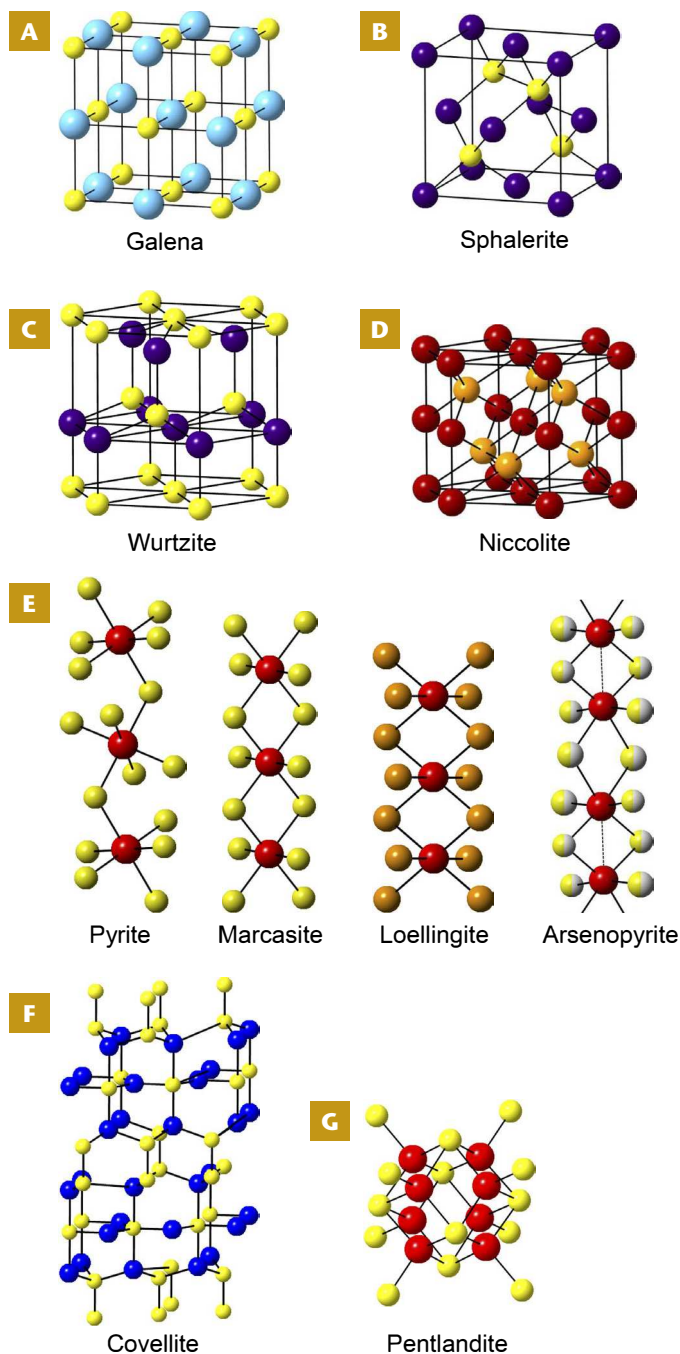
FIGURE 1 Crystal structures of the major sulfides. (**A**) Galena (PbS). (**B**) Sphalerite (ZnS). (**C**) Wurtzite (ZnS). (**D**) Niccolite (NiAs). (**E**) Linkage of metal–sulfur octahedra along the *c*-axis direction in pyrite (FeS_2), marcasite (FeS_2), loellingite ($FeAs_2$) and arsenopyrite (FeAsS). (**F**) Covellite (CuS). (**G**) Cube cluster of tetrahedrally coordinated metals in the pentlandite structure. Atom colours as follows: light blue – Pb; purple – Zn; yellow – S; red – Fe; orange – As; dark red – Ni; dark blue – Cu; for 1E arsenopyrite, yellow/grey spheres are either S or As. Adapted from Craig and Vaughan (1990).

In many of these groups, both the actual structure type (TABLE 1) and the other minerals 'derived' from these 'parent' structures are known. The relationship between derivatives and parents can involve:

1. **Distortion**, e.g. the troilite form of FeS, which is a distortion of the parent NiAs structure (FIG. 2A);

2. **Ordered omission**, e.g. monoclinic pyrrhotite (Fe_7S_8), which is derived from the NiAs structure of FeS by the removal of Fe atoms, so leaving vacancies that are ordered (FIG. 2A);

3. **Ordered substitution**, e.g. chalcopyrite ($CuFeS_2$) which is derived from sphalerite (ZnS) by the alternate replacement of Zn atoms by Cu and Fe, resulting in an enlarged (tetragonal) unit cell (FIG. 2B). Stannite (Cu_2FeSnS_4) results from further ordered substitution of half of the Fe atoms in chalcopyrite by Sn (FIG. 2B);

4. **Stuffed derivative**, e.g. talnakhite ($Cu_9Fe_8S_{16}$), mooihoekite ($Cu_9Fe_9S_{16}$) and haycockite ($Cu_4Fe_5S_8$), which are derived from chalcopyrite by the occupation of additional, normally empty, cavities in the structure (FIG. 2C).

CHEMISTRY OF SULFIDES

Bulk Composition

The chemical compositions of sulfide minerals have been well characterized by numerous analyses of natural samples and laboratory investigations of phase equilibria (TABLE 1 gives names and formulae of all common, and many less common, sulfides). Although most sulfide minerals are simple binary or ternary compounds, natural sulfides contain impurities ranging from trace (ppm) to minor (<5 wt%) amounts. Such impurities may include toxic elements such as arsenic, cadmium and mercury. The more extensive substitutions associated with solid solution are also found in the sulfides: for example, the complete solid solution between pyrite (FeS_2) and vaesite (NiS_2) to give the intermediate composition mineral bravoite [$(Fe,Ni)S_2$].

Certain sulfides also exhibit non-stoichiometry (deviation of the formula from an integral ratio). For example, pyrrhotite is commonly given the general formula $Fe_{1-x}S$ where $0 < x < 0.125$. The varying compositions correspond to varying concentrations of vacancies in iron atom sites. However, in systems such as these, ordering of the vacancies occurs at low temperatures, and the result may be a series of stoichiometric phases of slightly different compositions. Although Fe_7S_8 has a (monoclinic) superstructure that results from vacancy ordering (FIG. 2A), the situation in the so-called 'intermediate' or 'hexagonal' pyrrhotites is more complex. Some of these pyrrhotites may represent ordered phases with clearly defined compositions (Fe_9S_{10}, $Fe_{11}S_{12}$ and so on), but more complex and partial ordering in these systems may occur.

Experimental studies of the phase relations in sulfide systems have done much to inform our understanding of the crystallization of sulfides from melts and high-temperature fluids. Key binary systems that have been studied include Fe–S, Cu–S, Ni–S; ternary systems include Fe–Cu–S, Fe–Ni–S, Fe–Zn–S, and Fe–As–S. A few quaternary systems are particularly important, notably the Fe–Zn–As–S system. Details of the work done in these areas can be found in Vaughan and Craig (1978, 1997) and Fleet (2006). Phase diagrams derived using experimental data for the Fe–Cu–S system at 700°C and 300°C (after Vaughan and Craig 1997) are shown in FIGURE 3. At 700°C, melts are entirely crystallized, though two extensive solid solution fields are noteworthy: first, the intermediate solid solution (ISS) that includes chalcopyrite and other phases close to $CuFeS_2$ in composition; second, the field around bornite (bn). Further cooling to 300°C sees the shrinking of these fields and the associated separation by solid-state diffusion that produces the exsolution textures observed using reflected light microscopy (FIG. 3). In the example illustrated in FIGURE 3, exsolved chalcopyrite (yellow) occurs as
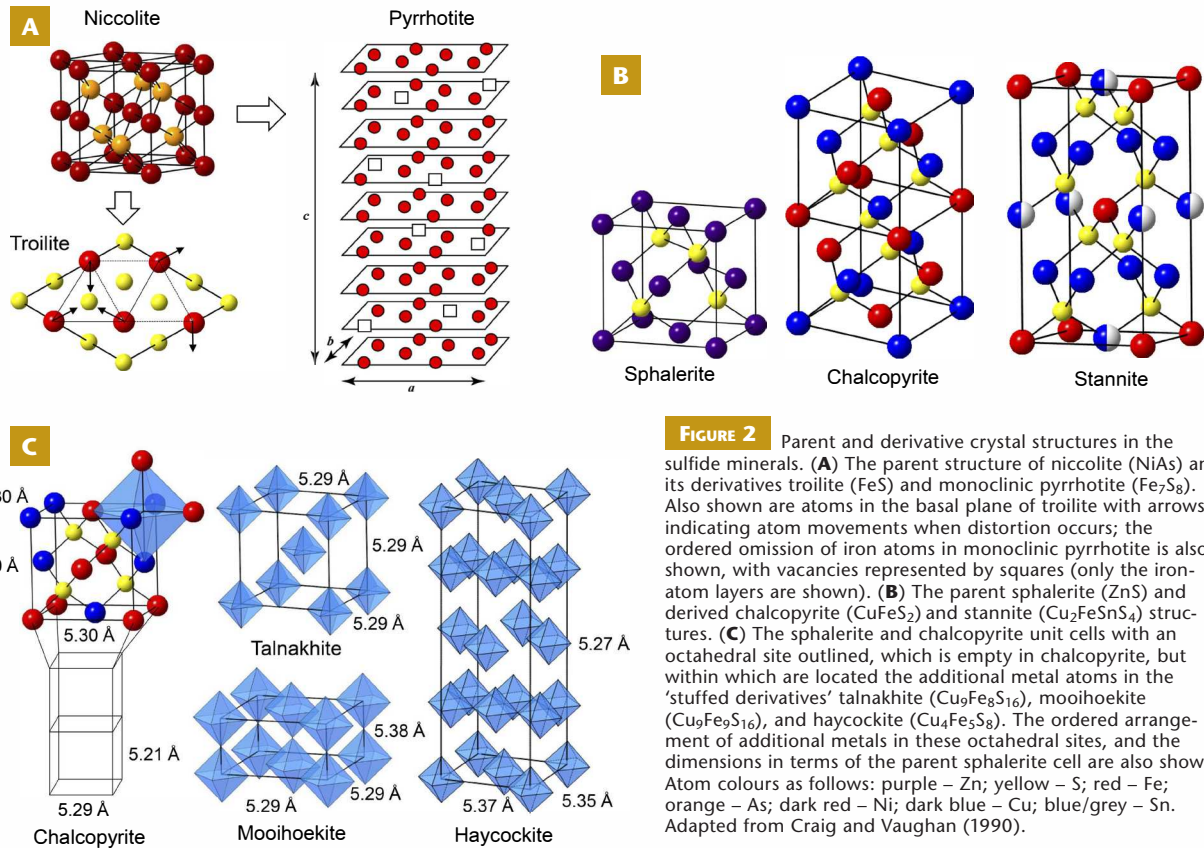
Figure 2 Parent and derivative crystal structures in the sulfide minerals. (**A**) The parent structure of niccolite (NiAs) and its derivatives troilite (FeS) and monoclinic pyrrhotite (Fe_7S_8). Also shown are atoms in the basal plane of troilite with arrows indicating atom movements when distortion occurs; the ordered omission of iron atoms in monoclinic pyrrhotite is also shown, with vacancies represented by squares (only the iron-atom layers are shown). (**B**) The parent sphalerite (ZnS) and derived chalcopyrite ($CuFeS_2$) and stannite (Cu_2FeSnS_4) structures. (**C**) The sphalerite and chalcopyrite unit cells with an octahedral site outlined, which is empty in chalcopyrite, but within which are located the additional metal atoms in the 'stuffed derivatives' talnakhite ($Cu_9Fe_8S_{16}$), mooihoekite ($Cu_9Fe_9S_{16}$), and haycockite ($Cu_4Fe_5S_8$). The ordered arrangement of additional metals in these octahedral sites, and the dimensions in terms of the parent sphalerite cell are also shown. Atom colours as follows: purple – Zn; yellow – S; red – Fe; orange – As; dark red – Ni; dark blue – Cu; blue/grey – Sn. Adapted from Craig and Vaughan (1990).

Table 1 SULFIDE MINERAL STRUCTURAL GROUPS. After Craig and Vaughan (1978)

Disulfide group				
Pyrite structure FeS_2 pyrite CoS_2 cattierite	*Marcasite structure* FeS_2 marcasite	*Arsenopyrite structure* FeAsS arsenopyrite FeSbS gudmundite	*Loellingite structure* $CoAs_2$ safflorite $FeAs_2$ loellingite $NiAs_2$ rammelsbergite	
Galena group				
PbS galena α-MnS alabandite				
Sphalerite group				
Sphalerite structure β-ZnS sphalerite CdS hawleyite Hg(S,Se) metacinnabar	*Derived by ordered substitution* $CuFeS_2$ chalcopyrite Cu_2FeSnS_4 stannite Cu_2ZnSnS_4 kesterite	*Stuffed derivatives* $Cu_9Fe_8S_{16}$ talnakhite $Cu_9Fe_9S_{16}$ mooihoekite $Cu_4Fe_5S_8$ haycockite		
Wurtzite group				
Wurtzite structure α-ZnS wurtzite CdS greenockite	*Composite structure derivatives* $CuFe_2S_3$ cubanite $AgFe_2S_3$ argentopyrite	*Derived by ordered substitution* Cu_3AsS_4 enargite		
Nickel arsenide group				
NiAs structure NiAs niccolite NiSb breithauptite	*Distorted derivatives* FeS troilite CoAs modderite	*Ordered omission derivatives* Fe_7S_8 monoclinic pyrrhotite Fe_9S_{10}, $Fe_{11}S_{12}$ hexagonal pyrrhotites		
Thiospinel group				
Thiospinel structure Co_3S_4 linnaeite $FeNi_2S_4$ violarite $CuCo_2S_4$ carrollite Fe_3S_4 greigite				
Layer sulfides group				
Molybdenite structure MoS_2 molybdenite WS_2 tungstenite	*Tetragonal PbO structure* FeS mackinawite ~Cu_3FeS_4 idaite	*Covellite structure* CuS covellite		
Metal excess group				
Pentlandite structure $(Ni,Fe)_9S_8$ pentlandite	*Argentite structure* Ag_2S argentite	*Chalcocite structure* Cu_2S chalcocite Ag_2S acanthite	*Digenite structure* Cu_9S_5 digenite Cu_5FeS_4 bornite	*Nickel sulfide structures* NiS millerite Ni_3S_2 heazlewoodite
Ring or chain structure group				
Stibnite structure Sb_2S_3 stibnite	*Realgar structure* As_4S_4 realgar	*Cinnabar structure* HgS cinnabar		

laths in host bornite (brown); the orientation of the laths is crystallographically controlled by the bornite host. The blue-grey phase is chalcocite, which was formed by later alteration of the bornite.

In another example, work on the Fe–As–S system has shown that the As content of arsenopyrite, when formed in equilibrium with pyrite and pyrrhotite, varies as a function of temperature and can be used as a geothermometer. On the other hand, work on the Fe–Zn–S system has demonstrated that increasing pressure reduces the iron content of sphalerite, and this can be used, under favourable circumstances, as a geobarometer.
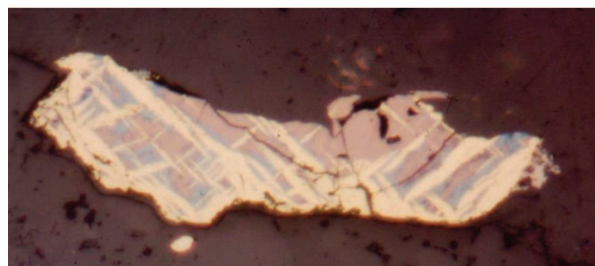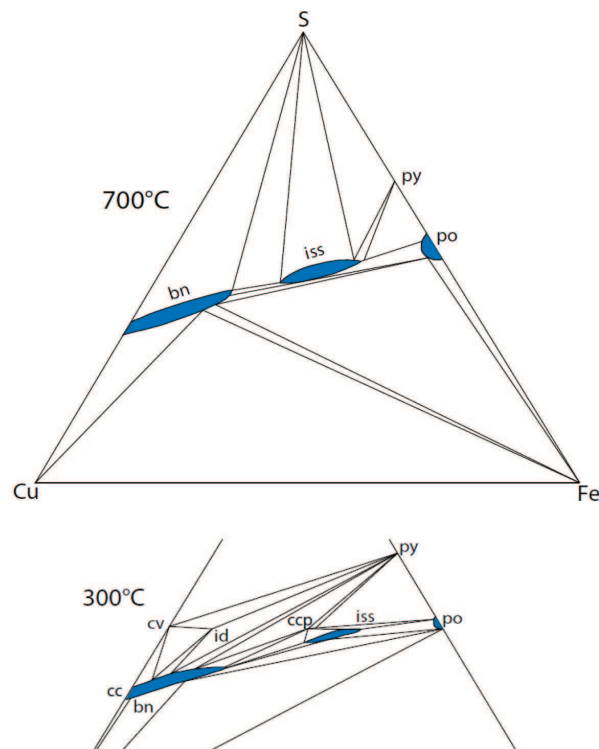

FIGURE 3 Phase relations in the Cu–Fe–S system at 700°C and 300°C. (**Upper**) Apart from the pure Cu, Fe, and S end-members, at 700°C, pyrite (py) is a stable phase and pyrrhotite (po) has a small area of solid solution coloured blue. There are two large fields of solid solution (also coloured blue), one centred around bornite (bn) and the other at the so-called intermediate solid solution (iss), which centres around chalcopyrite and related minerals. (**Middle**) On cooling to 300°C, all three solid solution fields decrease in area. New phases now stable are covellite (cv), chalcocite (cc) and idaite (id). Chalcopyrite (ccp) exsolves from the iss as it shrinks on cooling. (**Lower**) A reflected light microscopy image (width of field = 900 µm) showing crystallographically oriented chalcopyrite laths (yellow) now hosted by bornite (brown). The blue-grey areas are chalcocite alteration of the bornite. The sulfides are in a silicate mineral host and the sample is typical of a porphyry copper deposit (see TABLE 2).

Surface Chemistry

Sulfide surface chemistry is particularly important because of its relevance to the oxidation and breakdown of sulfide minerals and to the processing of mined ores using froth flotation or leaching. Investigations using spectroscopic and imaging studies of pristine surfaces in ultra-high vacuum (UHV) conditions have provided information on structure and reactivity at an atomic resolution. Micron-scale studies have investigated reacted surfaces and reaction products. Comprehensive reviews are provided by Rosso and Vaughan (2006a, b).

The most studied sulfide with respect to surface chemistry is pyrite. Pyrite's major surface crystallographic planes are (100), (111), (110) and (210), with the (100) surface considered the most stable. At the (100) surface, a complex microtopography has been observed in UHV, defined by flat, stepped terraces, commonly with a high step density (Rosso et al. 1999) (FIG. 4A, B). Spectroscopic studies of this surface in vacuum indicate that, upon cleavage, disulfide bonds break to form monosulfide species (Nesbitt et al. 1998; Schaufuß et al. 1998). The redox chemistry of pyrite in aqueous solution involves further complexities. Rimstidt and Vaughan (2003) note that oxidation of a disulfide, such as pyrite, to release sulfate requires transfer of seven electrons and, hence, up to seven elementary reaction steps. Furthermore, pyrite is a semiconductor, so the reactions are electrochemical in nature. This electrochemical reaction may involve three distinct steps: (1) cathodic reaction, (2) electron transport, and (3) anodic reaction. The cathodic reaction is probably the rate-determining step. The rate of pyrite oxidation may, thus, depend on the concentration of O_2 or an oxidant such as Fe^{3+}.

Sulfides such as monoclinic pyrrhotite (Fe_7S_8) also have complex surfaces. Superstructures within the pyrrhotite family arise from vacancy ordering in layers parallel to the basal plane (FIG. 2A). In the most Fe-deficient end-member, Fe vacancies occur in every other Fe atom layer and in alternate rows within that layer; in every S atom layer, one in four S atoms relaxes into an Fe vacancy. The (001) surface of monoclinic pyrrhotite was observed by scanning tunneling microscopy to comprise flat terraces separated by steps ~2.8 Å in height (FIG. 4C), which is one quarter of the unit cell in the c direction, or the separation between two consecutive Fe or S layers (Becker et al. 1997). Such complex surfaces then give rise to different oxidation mechanisms. Due to the deficiency in Fe atoms at the pyrrhotite surface, oxidation proceeds via the formation of a sulfur-rich layer (Chiriţă and Rimstidt 2014), whereas for the Fe-rich surface layers of pyrite, ferric oxyhydroxide forms during the initial oxidation.

There is significant environmental relevance in understanding the reactions at the surface of arsenopyrite during aqueous oxidation (see Corkhill and Vaughan 2009). Like pyrite oxidation, these are complex, multistage electrochemical reactions. Spectroscopic studies (Schaufuss et al. 2000; Corkhill et al. 2008) have shown that oxidation of As proceeds via a series of one-electron transfer steps, from As^{-1} to As^{5+}, with S oxidation considered as a 7-step reaction, transforming disulfide (S^{2-}) to sulfate sulfur (S^{6+}). Oxidation products, including ferric-(oxy)hydroxides, form an oxidized surface layer that is controlled by diffusion of species from the bulk mineral (Schaufuss et al. 2000; Costa et al. 2002). Oxidative leaching of arsenopyrite in the presence of common acid mine drainage bacteria (e.g. *Leptospirillum ferrooxidans*) greatly enhances the release of As from the surface when compared to abiotic dissolution. The mechanisms were a combination of direct leaching, as
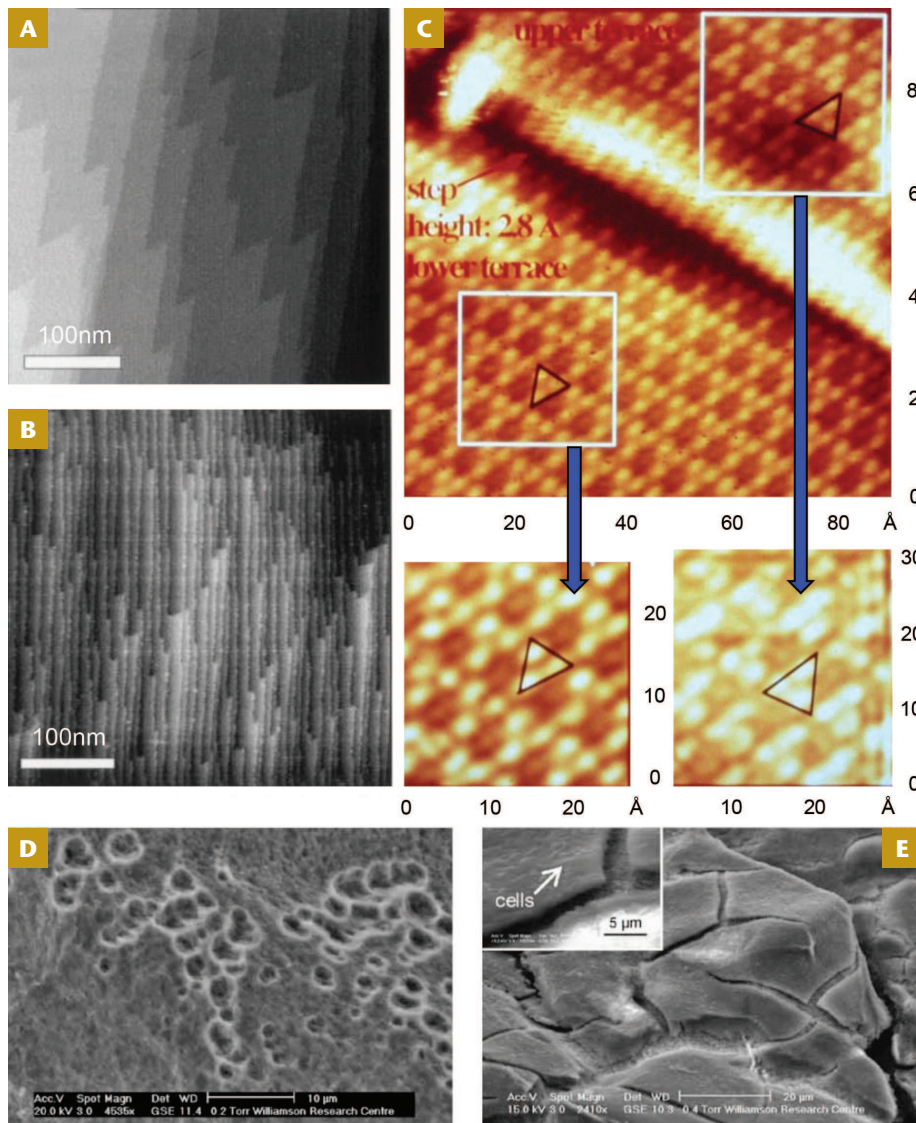
Images of sulfide surface structures. (**A**) Scanning tunneling microscope (STM) observation of large stepped (100) pyrite (FeS_2) terraces in the <10> direction. (**B**) Step terraces on pyrite commonly present at a high step density. After Rosso et al. (1999). (**C**) STM images of monoclinic pyrrhotite (Fe_7S_8), showing ~2.8 Å step height and triangles of groups of three S atoms in alternate directions of orientation on neighbouring layers across the 2.8 Å step. After Becker et al. (1997). (**D**) Bacterial leach pits on the surface of arsenopyrite (FeAsS) reacted in the presence of the acid mine drainage bacterium *Leptospirillum ferro-oxidans*, which were found below a layer of (**E**) extracellular polymeric substance, hypothesised to act as a dual direct and indirect oxidation mechanism for enhanced arsenic release. Figures 4D and 4E after Corkhill et al. (2008).

evidenced from cell-shaped etch pits (FIG. 4D), and indirect dissolution, through cycling of Fe^{2+} within a thick layer of extra-cellular polymeric substances (FIG. 4E).

The uptake of metal ions by sulfide surfaces is an important process in the transport and mobility of metals in the subsurface, in ore formation, and on the mobility of contaminants and other pollutants. Again, pyrite is the most studied phase, along with the readily studied galena cleavage surface and the environmentally important mackinawite (Rosso and Vaughan 2006b). Investigation of the sorption of heavy metals (e.g. As, Mo, Hg) and radionuclides (U, Tc) by pyrite surfaces has identified a number of complex reactions that lead to sorption. For example, in the sorption of Cd^{2+}, surface reconstruction and disproportionation occurs, leaving a mixture of sulfide and oxide products (Bostick et al. 2000). The problematic radionuclide ^{99}Tc was found sorbed to framboidal pyrite that was present in a clay formation that itself was used as host rock for the geological disposal of nuclear waste. The mechanism in this case was via oxidation–reduction, whereby Tc(IV)–sulfur-type phases were formed (Bruggeman et al. 2007).

PARAGENESIS OF SULFIDES

Sulfides in Ore Deposits

TABLE 2 shows the main types of ore deposits that contain significant amounts of sulfide minerals, their major ore minerals, the metals extracted from them, and some specific examples (see Cox and Singer 1987; Craig and Vaughan 1990, 1994). Pyrite is abundant in nearly all of these deposits. Notable exceptions are those ores found in association with intrusive ultramafic and mafic rocks, particularly the so-called 'sulfide nickel deposits', where the dominant sulfide mineral is pyrrhotite and it is associated with pentlandite and chalcopyrite. These latter minerals are regarded as having formed via crystallization from an immiscible sulfide melt that separated from the main silicate melt following injection into the country rock. In the Bushveld Igneous Complex (South Africa), the dominant sulfides are pyrrhotite, pentlandite and chalcopyrite. Crucially, from an economic perspective, some horizons, notably the 'Merensky Reef', are also enriched in platinum group minerals.

Pyrite is the dominant sulfide in porphyry copper deposits, though it is chalcopyrite that is the most important ore mineral, along with bornite and various binary copper sulfides. In the related porphyry molybdenum deposits, it is molybdenite that dominates. The sulfides in such deposits occur as veinlets or disseminated grains in host intrusions.

Type	Major Ore Minerals*	Metals Extracted	Examples
Ores related to mafic and ultramafic intrusions			
Sulfide nickel deposits	po, pn, py, cpy, viol	Ni, Cu, Co, PGM	Sudbury, Ontario, Canada
Merensky reef platinum	po, pn, cpy	Ni, Cu, PGM	Merensky Reef, RSA
Ores related to felsic intrusive rocks			
Tin and tungsten skarns	py, cass, sph, cpy, wf	Sn, W	Pine Creek, CA, USA
Zinc–lead skarns	py, sph, gn	Zn, Pb	Ban Ban, Australia
Copper skarns	py, cpy	Cu, Au	Carr Fork, Utah, USA
Porphyry copper/molybdenum	py, cpy, bn, mbd	Cu, Mo, Au	Bingham Canyon, Utah; USA Climax, CO, USA
Polymetallic veins	py, cpy, gn, sph, ttd	Cu, Pb, Zn, Ag	Camsell River, NWT, Canada
High sulfidation ores	py, enar, cov, ten, Au	Cu, Au, Ag	Summitville, CO, USA
Ores related to marine mafic extrusive rocks			
Cyprus-type massive sulfides	py, cpy	Cu	Cyprus
Besshi-type massive sulfides	py, cpy, sph, gn	Cu, Pb, Zn	Japan
Ores related to subaerial felsic to mafic extrusive rocks			
Creede-type epithermal veins	py, sph, gn, cpy, ttd, asp	Cu, Pb, Zn, Ag, Au	Creede, CO, USA
Ores related to marine felsic to mafic extrusive rocks			
Kuroko-type	py, cpy, gn, sph, ttd, asp	Cu, Pb, Zn, Ag, Au	Japan
Ores in clastic sedimentary rocks			
Quartz pebble U–gold	py, uran, gold	Au, U	Witwatsrand, RSA
Sandstone-hosted lead–zinc	py, sph, gn	Pb, Zn, Cd	Laisvall, Sweden
Sedimentary exhalative lead–zinc	py, sph, gn, cpy, asp, ttd, po	Cu, Pb, Zn, Au, Ag	Sullivan, BC, Canada Tynagh, Ireland
Ores in carbonate rocks			
Mississippi Valley type	py, gn, sph	Zn, Pb, Cd, Ga, Ge	Missouri, USA

* Abbreviations used are as follows: asp–arsenopyrite, Au–gold, bn–bornite, cass–cassiterite, cov–covellite, cpy–chalcopyrite, enar–enargite, gn–galena, mbd–molybdenite, PGM–platinum group minerals, pn–pentlandite, po–pyrrhotite, py–pyrite, sph–sphalerite, ten–tennantite, ttd–tetrahedrite, uran–uraninite, viol–violarite, wf–wolframite

Pyrite, along with sphalerite, galena or chalcopyrite, also occurs in large masses in the 'skarn' deposits formed by contact metamorphism, as a major phase in many hydrothermal vein deposits, and in those deposits that can be broadly described as 'volcanogenic'. Included in this latter group are ores that occur in thick volcanic sequences, such as the Kuroko-type deposits of Japan in which the 'black ore' contains irregular masses of galena intergrown with sphalerite, chalcopyrite and pyrite.

In the Besshi-type deposits, pyrite, chalcopyrite, sphalerite and galena are found in predominantly sedimentary sequences. Sulfide ores in volcano-sedimentary sequences, such as those associated with ophiolite complexes (e.g. the Troodos Complex in Cyprus) are dominated by pyrite and chalcopyrite. Our understanding of the formation of such deposits has been revolutionized by the study of present-day volcanic and hydrothermal activity on the seafloor. Disseminated to massive stratiform sulfide ores are often conformable within sedimentary sequences, grading into volcanic deposits of the kind discussed above. Pyrite again dominates the sulfide mineralogy in deposits such as those of the Copperbelt of Zambia, which have a range of copper–iron sulfides (chalcopyrite, bornite), copper sulfides (chalcocite, covellite) and significant amounts of cobalt in cobaltian pyrite and carrollite ($CuCo_2S_4$).

In ores associated with sedimentary rocks, sulfides (galena, sphalerite, pyrite) are major phases in the lead–zinc–barite–fluorite ores which occur mainly in limestones, most famously in the Mississippi Valley region (USA). Pyrite and various copper sulfides occur in the vanadium–copper ores that are associated with sandstones in the Colorado Plateau (USA), and in the gold–uranium deposits associated with conglomerates in Witwatsrand (South Africa). Pyrite and,

to a lesser extent, other sulfides, such as marcasite (FeS_2), are minor components in coals and accessory minerals in black shales.

Biogenic Formation of Sulfides

Sulfide minerals can also form through the activities of a group of bacteria known as dissimilatory sulfate-reducing prokaryotes (SRP) (see Rickard et al. 2017 this issue). The
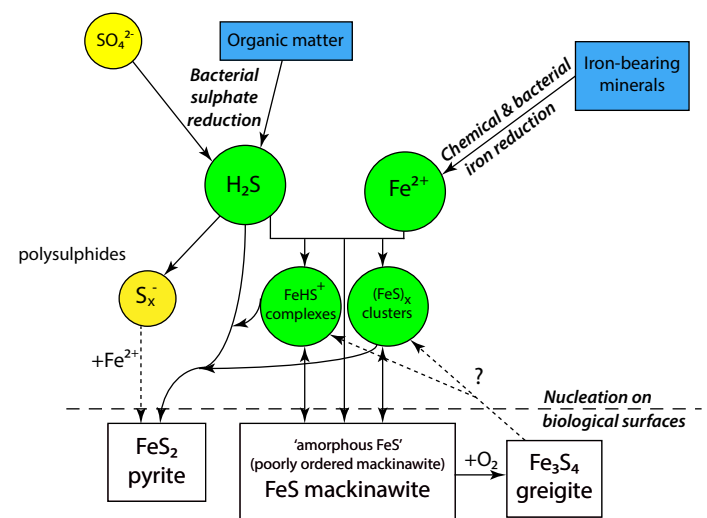
FIGURE 5 The pathways leading directly to the formation of pyrite or other iron sulfides (mackinawite and greigite) in the sedimentary environment. Information from Berner (1984), Lennie and Vaughan (1996) and Rickard and Morse (2005).

SRP occur in anaerobic environments that include lakes, swamps, soils and marine sediments. As part of their metabolic processes, these organisms reduce sulfate ions to sulfide which can react with any available dissolved metal ions to form highly insoluble sulfides. Other organisms may contribute to these processes through the microbial reduction of metals, particularly iron. Iron sulfide minerals generated in this way are ubiquitous in modern anoxic (particularly marine) sediments, and the pathways leading to their formation are illustrated in Figure 5. When the sulfide produced by SRP reacts with Fe^{2+}, a very fine particle black precipitate of poorly crystalline mackinawite (FeS) or a mixture of mackinawite and greigite (Fe_3S_4) is formed. These iron minerals are metastable and, with time, transform to pyrite. Three possible pathways for this transformation have been suggested (Fig. 5):

(1) FeS oxidation by a polysulfide
$$FeS + S_n^{2-} \rightarrow FeS_2 + S_{n-1}^{2-}$$

(2) FeS oxidation by H_2S
$$FeS + H_2S \rightarrow FeS_2 + H_2$$

(3) Conversion via a greigite phase
$$4FeS + \tfrac{1}{2}O_2 + 2H^+ \rightarrow Fe_3S_4 + Fe^{2+} + H_2O$$
$$Fe_3S_4 + 2H^+ \rightarrow 2FeS_2 + Fe^{2+} + H_2$$

Iron sulfide (FeS) 'nanoparticles' produced using SRP have a primary size of 1–2 nm; however, they are not stable and transform into highly crystalline nanorods with the structure of mackinawite within 48 hours (Hochella, pers comm). Xu et al. (2016) have shown that ZnS nanocrystals formed by SRP are distinctive from their abiogenic counterparts in morphology, crystal size, structural defects, dissolution behaviour and presence of the wurtzite form of ZnS.

Some organisms have evolved so as to synthesize sulfides for a particular biological function. One example is a deep-sea snail found around ocean floor hydrothermal vents, where parts of this animal's foot are covered by sulfide (pyrite and greigite) scales for structural support and protection against predators. Because of its magnetic (ferromagnetic) properties, greigite is also synthesized by certain magnetotactic bacteria. Here, intracellular greigite crystals form chains which can align with the Earth's magnetic field to enable the organism to find its optimal position in its environment. The subject of sulfides in biosystems has been reviewed by Pósfai and Dunin-Borkowski (2006).

A great deal is now known about the compositions, crystal structures, phase relations and parageneses of sulfide minerals. But there is still much work to be done on their surface chemistry, surface reactivity, biogeochemistry and, in particular, in the study of sulfide nanoparticles. ◾

REFERENCES

Becker U, Munz AW, Lennie AR, Thornton G, Vaughan DJ (1997) The atomic and electronic structure of the (001) surface of monoclinic pyrrhotite (Fe_7S_8) as studied using STM, LEED and quantum mechanical calculations. Surface Science 389: 66-87

Berner RA (1984) Sedimentary pyrite formation; an update. Geochimica et Cosmochimica Acta 48: 605-615

Bostick BC, Fendorf S, Fendorf M (2000) Disulfide disproportionation and CdS formation upon cadmium sorption on FeS_2. Geochimica et Cosmochimica Acta 64: 274-255

Bowles JFW, Howie RA, Vaughan DJ, Zussman J (2011) Non-silicates: Oxides, Hydroxides and Sulphides. Rock-Forming Minerals Vol. 5A, Geological Society, London. 920 pp

Bruggeman C, Maes A, Vancluysen J (2007) The identification of FeS_2 as a sorption sink for Tc(IV). Physics and Chemistry of the Earth 32: 573-580

Chiriță P, Rimstidt JD (2014) Pyrrhotite dissolution in acidic media. Applied Geochemistry 41: 1-10

Corkhill CL, Vaughan DJ (2009) Arsenopyrite oxidation – a review. Applied Geochemistry 24: 2342-2361

Corkhill CL, Wincott PL, Lloyd JR, Vaughan DJ (2008) The oxidative dissolution of arsenopyrite (FeAsS) and enargite (Cu_3AsS_4) by *Leptospirillum ferrooxidans*. Geochimica et Cosmochimica Acta 72: 5616-5633

Costa MC, Botelho de Rogo AM, Abrantes LM (2002) Characterization of a natural and an electro-oxidized arsenopyrite: a study on electrochemical and X-ray photoelectron spectroscopy. International Journal of Mineral Processing 65: 83-108

Cox DP, Singer DA (eds) (1987) Mineral Deposit Models. US Geological Survey Professional Paper 1693

Craig JR, Vaughan DJ (1990) Compositional and textural variations of the major iron and base-metal suphide minerals. In: Gray PMJ, Bowyer GJ, Castle JF, Vaughan DJ, Warner NA (eds). Sulphide Deposits—Their Origin and Processing. Institution of Mining and Metallurgy, London, pp 1-16

Craig JR, Vaughan DJ (1994) Ore Microscopy and Ore Petrography. 2nd Edition. Wiley-Interscience, New York, 368 pp

Fleet ME (2006) Phase equilibria at high temperatures. Reviews in Mineralogy and Geochemistry 61: 365-419

Lennie AR Vaughan DJ (1996) Spectroscopic studies of iron sulfide formation and phase relations at low temperatures. In: Dyar MD, McCammon C, Schafer MW (eds) Mineral Spectroscopy: A Tribute to Roger G. Burns. Geochemical Society, Special Publication 5, pp 117-131

Makovicky E (2006) Crystal structures of sulfides and other chalcogenides. Reviews in Mineralogy and Geochemistry 61: 7-125

Nesbitt HW, Bancroft GM, Pratt AR, Scaini MJ (1998) Sulfur and iron surface states on fractured pyrite surfaces. American Mineralogist 83: 1067-1076

Pósfai M, Dunin-Borkowski RE (2006) Sulfides in Biosystems. Reviews in Mineralogy and Geochemistry 61: 679-714

Ribbe PH (ed) (1974) Sulfide Mineralogy. Mineralogical Society of America Short Course Notes, Volume 1. Mineralogical Society of America, Chantilly, 301 pp

Rickard D, Mussmann M, Steadman, JA (2017) Sedimentary sulfides. Elements 13: 119-124

Rickard DT, Morse JW (2005) Acid volatile sulfide (AVS). Marine Chemistry 97: 141-197

Rimstidt JD, Vaughan DJ (2003) Pyrite oxidation: a state-of-the-art assessment of the reaction mechanism. Geochimica et Cosmochimica Acta 67: 873-880

Rosso KM, Becker U, Hochella MF (1999) Atomically resolved electronic structure of pyrite {100} surfaces: an experimental and theoretical investigation with implications for reactivity. American Mineralogist 84: 1535-1548

Rosso KM, Vaughan DJ (2006a) Sulphide mineral surfaces. Reviews in Mineralogy and Geochemistry 61: 505-556

Rosso KM, Vaughan DJ (2006b) Reactivity of sulfide mineral surfaces. Reviews in Mineralogy and Geochemistry 61: 557-608

Schaufuß AG and 5 coauthors (1998) Reactivity of surface chemical states on fractured pyrite. Surface Science 411: 321-328

Schaufuss AG and 5 coauthors (2000) Reactivity of surface chemical states on fractured arsenopyrite (FeAsS) toward oxygen. American Mineralogist 85: 1754-1766

Vaughan DJ (ed) (2006) Sulfide Mineralogy and Geochemistry. Reviews in Mineralogy and Geochemistry, Volume 61. Mineralogical Society of America, 714 pp

Vaughan DJ, Craig JR (1978) Mineral Chemistry of Metal Sulfides. Cambridge University Press, Cambridge, 512 pp

Vaughan DJ, Craig JR (1997) Sulfide ore mineral stabilities, morphologies, and intergrowth textures. In: Barnes HL (ed) Geochemistry of Hydrothermal Ore Deposits. 3rd edition. Wiley-Interscience, New York, pp 367-434

Xu J and 7 coauthors (2016) Highly defective nanocrystals of zinc sulfide produced via dissimilatory bacterial sulfate reduction: a comparative study with abiogenic analogues. Geochimica et Cosmochimica Acta 180: 1-14 ◾

Break Boundaries with SELFRAG